SHEAR WAVE SCATTERING FROM A DEBONDED FIBRE

Y. YANG and A. N. NORRIS

Department of Mechanics and Materials Science, Rutgers University, P.O. Box 909, Piscataway, NJ 08855-0909, U.S.A.

(Received 3 August 1989; in revised form 15 January 1990)

ABSTRACT

SCATTERING of an antiplane shear wave from a single fibre partially bonded to a matrix is considered. The region of debonding is modeled as an interface crack with non-contacting faces; the crack opening displacement is represented by Chebyshev polynomials, and a system of equations is derived for the unknown coefficients. The solution is valid for arbitrary values of k_1a , where k_1 is the incident wavenumber and a the fibre radius, and the semi-angle δ subtended by the crack may vary from zero to π . The general solution simplifies in two limiting situations: (i) if δ is small, and $k_1a\delta$ is also small, then the wavelength greatly exceeds the crack length and the crack is effectively subject to a static loading determined by the dynamic field around the perfectly bonded fibre. Explicit expressions can be obtained for the COD and the scattered field in this case; (ii) when the crack semi-angle is finite, but k_1a is small, then both the field in the fibre and the crack loading are quasistatic. The dependence of the scattered field on δ is particularly simple; however, the quasistatic theory breaks down at surprisingly low values of k_1a when the fibre becomes almost completely separated from the matrix. The narrow neck joining the matrix and fibre permits the fibre to oscillate at very low frequencies and causes a strong resonance in the scattering crosssection. The general and approximate results for the single fibre are used to estimate the attentuation of a wave propagating through a composite with many fibres and the possibility of quantitative detection of debonding using ultrasound attenuation measurements is discussed.

1. INTRODUCTION

The Partial debonding of fibres in reinforced composites can be the precursor to serious degradation of mechanical properties. Thus, if a large enough axial load is applied, the fibres may completely disengage from the matrix, possibly resulting in catastrophic failure. The topic of this paper is the effect of debonding on the scattering of antiplane shear waves. The solution to this problem is relevant to ultrasonic nondestructive detection of debonding, and could have applications to the question of how dynamic loading can lead to growth of debonds. The solution may also be of interest to earthquake engineers concerned with the motion of foundation piles. The associated long wavelength or quasistatic problem has been solved in closed form by Coussy (1982, 1986). However, as we will see, the values of dimensionless frequency, ka, for which the quasistatic solution is valid may be strictly limited to $ka \ll 1$, and it could break down at values for which it might otherwise be expected to hold.

The present method of solution is similar to that of Krenk and Schmidt (1982) who considered the scattering of elastic waves from a penny-shaped crack in a

homogeneous medium. Their method was also used by Boström (1987) in solving for the SH scattered field due to an interface crack between two homogeneous elastic half spaces. The two problems discussed by Boström (1987) and in the present paper are simpler than the fully elastic problem of in-plane longitudinal and shear wave incidence (Coussy, 1984) in that the crack opening displacement on the debond has the usual square root behaviour near the edges. However, the technique outlined here could be extended to the in-plane problem, although the algebra is necessarily quite a bit more extensive, and will be discussed in a later paper. As Boström (1987) noted, the present method does not involve the use of Green's functions. This is a tremendous simplification and leads to the ultimate equations in a direct and straightforward manner.

2. FORMULATION AND SOLUTION OF THE PROBLEM

2.1. Decomposition into symmetric and antisymmetric parts

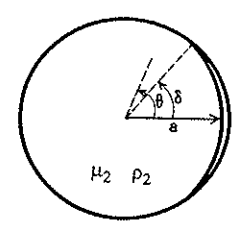
Let the shear modulus and mass density of the matrix and fibre be μ_1 , ρ_1 , and μ_2 , ρ_2 , respectively. The fibre occupies r < a, the matrix r > a, and polar coordinates (r, θ) will be used. All motion is time harmonic of frequency ω , and the term $e^{-i\omega t}$ will be omitted, but understood. Let the interface crack be of angular width 2δ , and centred at $\theta = 0$, see Fig. 1. The total out-of-plane displacement is expressed as

$$u^{\text{tot}}(r,\theta) = \begin{cases} u^{\text{in}} + u_1^{(0)} + u_1^{(1)}, & r > a, \\ u_2^{(0)} + u_2^{(1)}, & r < a, \end{cases}$$
 (2.1)

where $u^{\rm in}$ represents the incident wavefield, $u_1^{(0)}$ and $u_2^{(0)}$ are the fields that would be present if the fibre were perfectly bonded, and $u_1^{(1)}$ and $u_2^{(1)}$ are the additional fields generated by the debond. All these fields, except possibly $u^{\rm in}$ which could possess singularities, are homogeneous solutions to the wave equation in their respective regions,

$$\nabla^2 u + k_\alpha^2 u = 0, \quad \alpha = \begin{cases} 1, & r > a, \\ 2, & r < a. \end{cases}$$
 (2.2)

where



 μ_1 ρ_1



Fig. 1. The partially debonded fibre and the incident wave direction.

Shear wave scattering from a debonded fibre

$$k_z = \omega/c_z,\tag{2.3}$$

$$c_{\alpha} = (\mu_{\alpha}/\rho_{\alpha})^{1/2}.$$
 (2.4)

The determination of the fields $u_x^{(0)} \alpha = 1$, 2, is a standard problem, with solutions given in Appendix A for the incident plane wave

$$u^{\rm in} = A e^{ik_1 r \cos(\theta - \theta_0)}, \tag{2.5}$$

propagating in the θ_0 direction. In order to solve for the additional fields $u_{\alpha}^{(1)}$, $\alpha = 1$, 2, it is helpful to decompose the fields as

$$u_{\alpha}^{(1)} = u_{\alpha S}^{(1)} + u_{\alpha A}^{(1)}, \quad \alpha = 1, 2,$$
 (2.6)

where $u_{\rm aS}^{(1)}$ and $u_{\rm aA}^{(1)}$ are symmetric and antisymmetric, respectively, about the line $\theta = 0$. A symmetric function $h_{\rm S}(r,\theta)$ satisfies

$$h_{\rm S}(r,\theta) = h_{\rm S}(r,2\pi - \theta), \quad 0 \leqslant \theta \leqslant \pi,$$
 (2.7)

while for an antisymmetric function, h_{Λ} ,

$$h_{\Lambda}(r,\theta) = -h_{\Lambda}(r,2\pi - \theta), \quad 0 \le \theta < \pi.$$
 (2.8)

2.2. The symmetric solution

Since the solution satisfies the symmetry condition (2.7) by definition, we need only consider the half plane, $r \ge 0$, $0 \le \theta \le \pi$. The interface conditions for the displacement and stress are

$$u_{1S}^{(1)} - u_{2S}^{(1)} = \begin{cases} 0, & r = a, \quad \delta \leqslant \theta \leqslant \pi, \\ \Delta U_{S}(\theta), & r = a, \quad 0 \leqslant \theta < \delta, \end{cases}$$
(2.9)

$$\mu_1 \frac{\partial u_{1S}^{(1)}}{\partial r} = \mu_2 \frac{\partial u_{2S}^{(1)}}{\partial r}, \quad r = a, \quad 0 \leqslant \theta \leqslant \pi, \tag{2.10}$$

where $\Delta U_{\rm S}(\theta)$ is the symmetric crack opening displacement (COD).

The scattered fields due to the presence of the crack must satisfy the Helmholtz equation (2.2) and be symmetric. Therefore, referring to Appendix A, let

$$u_{1S}^{(i)} = \sum_{n=0}^{\infty} E_n^{(S)} H_n^{(i)}(k_1 r) \cos n\theta, \qquad (2.11a)$$

$$u_{2S}^{(1)} = \sum_{n=0}^{\infty} F_n^{(S)} J_n(k_2 r) \cos n\theta, \qquad (2.11b)$$

which when substituted into (2.10) yield

$$E_n^{(S)} = Z \frac{J_n'(k_2 a)}{H_n^{(1)'}(k_1 a)} F_n^{(S)},$$
 (2.12)

where Z is defined in (A6) Eliminating $E_n^{(S)}$ in favour of $F_n^{(S)}$, and using (2.9), (2.10) and (A5) gives

$$\sum_{n=0}^{\infty} F_n^{(S)} \frac{D_n}{H_n^{(1)'}(k_1 a)} \cos n\theta = \begin{cases} 0, & \delta \leqslant \theta \leqslant \pi, \\ -\Delta U_S(\theta), & 0 \leqslant \theta < \delta, \end{cases}$$
(2.13)

and therefore

$$F_n^{(S)} = -\frac{\varepsilon_n}{\pi} \frac{H_n^{(1)'}(k_1 a)}{D_n} \int_0^\delta \Delta U_S(\theta) \cos n\theta \, d\theta, \qquad (2.14)$$

where ε_n and D_n , n = 0, 1, 2, ..., are defined in Appendix A.

So far, we have not required the total stress to vanish on the crack faces. This condition is, for the symmetric solution,

$$\frac{\partial u_{2s}^{(0)}}{\partial r} + \frac{\partial u_{2s}^{(1)}}{\partial r} = 0, \quad r = a, \quad 0 \le \theta < \delta, \tag{2.15}$$

where $u_{2S}^{(0)}$ is the symmetric part of $u_2^{(0)}$, which may be expressed as

$$u_{2S}^{(0)} = \sum_{n=0}^{\infty} B_n^{(S)} J_n(k_2 r) \cos n\theta.$$
 (2.16)

The coefficients $B_n^{(S)}$, n = 0, 1, 2, ..., depend upon the type of incident wave considered, and are given in Appendix A for an incident plane wave. Substituting (2.11b), (2.14) and (2.16) into (2.15) yields

$$\sum_{p=0}^{\infty} \frac{\varepsilon_p}{\pi} \cos p\theta J_{\rho}'(k_2 a) \frac{H_{\rho}^{(1)'}(k_1 a)}{D_{\rho}} \int_0^{\delta} \Delta U_{S}(\psi) \cos p\psi \,d\psi$$

$$= \sum_{p=0}^{\infty} B_{\rho}^{(S)} J_{\rho}'(k_2 a) \cos p\theta, \quad 0 \le \theta < \delta. \quad (2.17)$$

We next expand the symmetric COD in a complete set of Chebyshev functions,

$$\Delta U_{\rm S}(\theta) = \sum_{n=1}^{\infty} \alpha_n^{\rm (S)} \phi_n^{\rm (S)}(\theta), \qquad (2.18)$$

where

$$\phi_n^{(S)}(\theta) = \frac{1}{2n-1} \cos \left[(2n-1) \arcsin \left(\frac{\theta}{\delta} \right) \right]. \tag{2.19}$$

These functions have the desired square root behaviour near the crack edge, $\theta = \delta$, and have been used previously in related problems (NEERHOFF, 1979; BOSTRÖM, 1987). The integrals in (2.17) may be expanded in terms of the COD coefficients $\alpha_n^{(S)}$ by using

$$\int_{0}^{\delta} \phi_{n}^{(S)}(\theta) \cos p\theta \, d\theta = \begin{cases} \frac{\pi}{2p} J_{2n-1}(p\delta), & p = 1, 2, 3, \dots, \\ \frac{\pi\delta}{4} \delta_{n1}, & p = 0, \end{cases}$$
 (2.20)

where $\delta_{mn} = 1$ if m = n, 0 if $m \neq n$. Then multiplying (2.17) by $\phi_m^{(S)}(\theta)$ and integrating

yields a system of linear equation for the COD coefficients,

$$\sum_{n=1}^{\infty} Q_{nm}^{(S)} \alpha_n^{(S)} = N_m^{(S)}, \quad m = 1, 2, 3, \dots,$$
 (2.21)

where the symmetric, complex-valued matrix $[Q^{(S)}]$ has elements

$$Q_{mn}^{(S)} = \frac{\delta^{2}}{8} \delta_{m1} \delta_{n1} \frac{H_{0}^{(1)'}(k_{1}a) J_{0}'(k_{2}a)}{D_{0}} + \sum_{p=1}^{\infty} \frac{1}{p^{2}} J_{2m-1}(p\delta) J_{2n-1}(p\delta) \frac{H_{p}^{(1)'}(k_{1}a) J_{p}'(k_{2}a)}{D_{p}}$$
(2.22)

and

$$N_n^{(S)} = \frac{\delta}{2} \delta_{n1} J_0'(k_2 a) B_0^{(S)} + \sum_{p=1}^{\infty} \frac{B_p^{(S)}}{p} J_{2n-1}(p\delta) J_p'(k_2 a). \tag{2.23}$$

Having solved (2.21) for the COD coefficients, the symmetric part of the scattered field due to the debond follows from (2.11a), (2.12), (2.14), (2.18) and (2.20) as

$$u_{1S}^{(1)} = -\frac{\delta}{4} \alpha_{1}^{(S)} Z \frac{J'_{0}(k_{2}a)}{D_{0}} H_{0}^{(1)}(k_{1}r)$$

$$-\sum_{n=1}^{\infty} \frac{ZJ'_{n}(k_{2}a)}{nD_{n}} H_{n}^{(1)}(k_{1}r) \cos n\theta \sum_{q=1}^{\infty} \alpha_{q}^{(S)} J_{2q-1}(n\delta). \quad (2.24)$$

This becomes in the far-field

$$u_{1S}^{(1)} \sim \left(\frac{8\pi}{k_1 r}\right)^{1/2} e^{i(k_1 r - \pi/4)} F_{S}^{(1)}(\theta, \theta_0),$$
 (2.25)

where the symmetric part of the far-field pattern is

$$F_{S}^{(1)}(\theta,\theta_{0}) = \frac{-Z}{2\pi} \left\{ \frac{\delta J_{0}(k_{2}a)}{4 D_{0}} \alpha_{1}^{(S)} + \sum_{n=1}^{\infty} \frac{(-i)^{n} J_{n}'(k_{2}a)}{nD_{n}} \cos n\theta \sum_{q=1}^{\infty} \alpha_{q}^{(S)} J_{2q-1}(n\delta) \right\}.$$
 (2.26)

2.3. The antisymmetric solution

Define the antisymmetric COD, $\Delta U_{\rm A}(\theta)$, by the interface condition analogous to (2.9),

$$u_{1A}^{(1)} - u_{2A}^{(1)} = \begin{cases} 0, & r = a, & \delta \leq \theta < \pi, \\ \Delta U_{\Lambda}(\theta), & r = a, & 0 \leq \theta < \delta. \end{cases}$$
 (2.27)

Then it is possible using the same procedures as before to obtain an equation for $\Delta U_{\rm A}$,

$$\sum_{\rho=1}^{\infty} \frac{2}{\pi} \sin p\theta J_{\rho}'(k_2 a) \frac{H_{\rho}'(k_1 a)}{D_{\rho}} \int_{0}^{\delta} \Delta U_{\rm A}(\psi) \sin p\psi \, \mathrm{d}\psi$$

$$= \sum_{p=1}^{\infty} B_p^{(\Lambda)} J_p'(k_2 a) \sin p\theta, \quad 0 \le \theta < \delta, \quad (2.28)$$

where the coefficients $B_n^{(A)}$, n = 1, 2, ..., are defined by

$$u_{2A}^{(0)} = \sum_{n=1}^{\infty} B_n^{(A)} J_n(k_2 r) \sin n\theta.$$
 (2.29)

Explicit expressions are given for $B_n^{(A)}$ in Appendix A for an incident plane wave. As before, expand the COD in a complete set of antisymmetric Chebyshev functions,

$$\Delta U_{\Lambda}(\theta) = \sum_{n=1}^{\infty} \alpha_n^{(\Lambda)} \phi_n^{(\Lambda)}(\theta), \qquad (2.30)$$

where

$$\phi_n^{(\Lambda)}(\theta) = \frac{1}{2n} \sin \left[2n \arcsin\left(\frac{\theta}{\delta}\right) \right].$$
 (2.31)

These have the property that

$$\int_0^\delta \phi_n^{(\Lambda)}(\theta) \sin p\theta \, \mathrm{d}\theta = \frac{\pi}{2p} J_{2n}(p\delta), \quad p = 1, 2, 3, \dots$$
 (2.32)

Substituting (2.30) into (2.28), multiplying both sides of (2.28) by $\phi_m^{(A)}(\theta)$ and integrating yields the system of equations

$$\sum_{n=1}^{\infty} Q_{mn}^{(\Lambda)} \alpha_n^{(\Lambda)} = N_m^{(\Lambda)}, \quad m = 1, 2, 3, \dots,$$
 (2.33)

where

$$Q_{nm}^{(\Lambda)} = \sum_{p=1}^{\infty} \frac{1}{p^2} J_{2m}(p\delta) J_{2n}(p\delta) \frac{H_p^{(1)'}(k_1 a) J_p'(k_2 a)}{D_p},$$
(2.34)

$$N_n^{(\Lambda)} = \sum_{p=1}^{\infty} \frac{B_p^{(\Lambda)}}{p} J_{2n}(p\delta) J_p'(k_2 a). \tag{2.35}$$

Once the α_n^A , n = 1, 2, 3, ..., have been determined the antisymmetric part of the scattered far-field pattern follows as

$$F_{\Lambda}^{(1)}(\theta,\theta_0) = -\frac{Z}{2\pi} \sum_{n=1}^{\infty} (-i)^n \frac{J'_n(k_2 a)}{nD_n} \sin n\theta \sum_{q=1}^{\infty} \alpha_q^{(\Lambda)} J_{2q}(n\delta).$$
 (2.36)

3. SCATTERING CROSS-SECTION AND ATTENUATION

The scattered far-field may be written

$$u^{\text{sc}} = u^{\text{tot}} - u^{\text{in}} \sim \left(\frac{8\pi}{k_1 r}\right)^{1/2} e^{i(k_1 r - \pi/4)} F(\theta, \theta_0),$$
 (3.1)

where the radiation pattern is

Shear wave scattering from a debonded fibre

$$F(\theta, \theta_0) = F^{(0)}(\theta, \theta_0) + F_S^{(1)}(\theta, \theta_0) + F_A^{(1)}(\theta, \theta_0). \tag{3.2}$$

The pattern $F^{(0)}$ is that for the perfectly bonded cylinder, and is given in Appendix A for plane wave incidence. The total energy flux for the scattered field is the time average of the flux over any surface S enclosing the cylinder,

$$\langle P \rangle = \frac{\omega}{2} \operatorname{Im} \int_{S} \mu_{1} \overline{u^{\text{sc}}} \frac{\partial u^{\text{sc}}}{\partial n} dS$$

$$= 4\pi \omega \mu_{1} \int_{0}^{2\pi} |F(\theta, \theta_{0})|^{2} d\theta. \tag{3.3}$$

The latter integral can be evaluated using the two-dimensional optical theorem,

$$\int_0^{2\pi} |F(\theta, \theta_0)|^2 d\theta = -\operatorname{Re} \bar{A} F(\theta_0, \theta_0). \tag{3.4}$$

The total scattering cross-section σ is defined as $\langle P \rangle$ divided by the time average of the incident flux,

$$\sigma(\omega) = \frac{\langle P \rangle}{\frac{\omega}{2} \mu_1 k_1 |A|^2}.$$
 (3.5)

Let $\sigma^{(0)}(\omega)$ be the cross-section for the perfectly bonded fibre. Then using the optical theorem (3.4), we have

$$\sigma(\omega) = \sigma^{(0)} - \frac{8\pi}{k_1 |A|^2} \operatorname{Re} \bar{A} F^{(1)}(\theta_0, \theta_0), \tag{3.6}$$

where $F^{(1)}$ is the sum of $F_S^{(1)}$ and $F_A^{(1)}$.

Consider, for simplicity, a composite of aligned identical fibres in a matrix such that there are N fibres per unit area in the plane perpendicular to the fibre axis. Let each fibre be partially debonded, with the same size crack and orientation on all the fibres. Distributions of crack sizes and orientations could be considered by a simple extension. The effect of each fibre is to scatter energy from the coherent wave propagating through the composite medium, resulting in attenuation of magnitude $\alpha = \text{Im } (k)$, where k is the complex-valued coherent wave number. The simplest way to approximate α is by neglecting multiple scattering effects, which gives the estimate

$$\alpha = \frac{N}{2}\sigma$$

$$= \frac{c\sigma}{2\pi a^2},$$
(3.7)

where c is the volume fraction of fibres in the composite. Thus, the effect of the debonding on the attenuation of the coherent wave may be estimated from (3.6) and (3.7). In particular, let $\alpha^{(0)}$ be the attenuation in the absence of debonding. Then the relative change in attenuation due to debonding is

$$\frac{\Delta \alpha}{\alpha^{(0)}} = \frac{\operatorname{Re} \bar{A} F^{(1)}(\theta_0, \theta_0)}{\operatorname{Re} \bar{A} F^{(0)}(\theta_0, \theta_0)}.$$
(3.8)

The approximation which led to (3.7) and (3.8) considers each fibre as isolated in an otherwise homogeneous material and neglects the interaction between fibres, which may in fact be of equal importance to the scattering from an individual fibre.

4. THE LONG WAVELENGTH LIMIT

4.1. General solution

The solution simplifies somewhat in the limit that the incident wavelength greatly exceeds the fibre radius, i.e. $k_1a \ll 1$. It is also assumed that $k_2/k_1 = O(1)$, or $k_2a = O(k_1a)$. This limit is equivalent to a static loading of the fibre, and so it may also be called the quasistatic limit.

First, we note that the matrices $[Q^{(S)}]$ and $[Q^{(A)}]$ of (2.22) and (2.34) become

$$[Q^{(T)}] = \frac{1}{k_2 a \left(1 + \frac{\mu_2}{\mu_1}\right)} [\tilde{Q}^{(T)}] + O(1), \quad T = S, A, \tag{4.1}$$

where $[\tilde{Q}^{(S)}]$ and $[\tilde{Q}^{(A)}]$ are symmetric, real-valued matrices that depend only upon δ ,

$$\widetilde{Q}_{nm}^{(S)} = \sum_{n=1}^{\infty} \frac{1}{p} J_{2m-1}(p\delta) J_{2n-1}(p\delta), \tag{4.2a}$$

$$\widetilde{Q}_{mn}^{(\Lambda)} = \sum_{p=1}^{\infty} \frac{1}{p} J_{2m}(p\delta) J_{2n}(p\delta). \tag{4.2b}$$

When the incident wave is a plane wave, see Appendix A, the COD coefficients become, for n = 1, 2, 3, ...,

$$\alpha_n^{(S)} = 2ik_1 a \cos \theta_0 \tilde{\alpha}_n^{(S)} A + O((k_1 a)^2), \tag{4.3a}$$

$$\alpha_n^{(A)} = 2ik_1 a \sin \theta_0 \tilde{\alpha}_n^{(A)} A + O((k_1 a)^2),$$
 (4.3b)

where $\tilde{\alpha}^{(S)}$ and $\tilde{\alpha}^{(A)}$ are real-valued and also depend only upon δ . They satisfy

$$\sum_{n=1}^{\infty} \tilde{Q}_{mn}^{(S)} \tilde{\alpha}_{n}^{(S)} = J_{2m-1}(\delta), \quad m = 1, 2, 3, \dots,$$
 (4.4a)

$$\sum_{n=1}^{\infty} \tilde{Q}_{mn}^{(A)} \tilde{\alpha}_{n}^{(A)} = J_{2m}(\delta), \quad m = 1, 2, 3, \dots,$$
 (4.4b)

which follow from (A4b), (2.23), (2.35) and (4.1)–(4.3). We note from (4.3) that the COD is of order (k_1a) in magnitude, it is in-phase with the incident stress field, and has a simple dependence upon the incident direction; all of which one could surmise independently from quasistatic arguments.

4.2. The radiated field and the limit of $\delta \rightarrow \pi$

The radiation pattern in the absence of any debonding becomes in the long wavelength limit

$$F^{(0)}(\theta, \theta_0) = A \frac{i}{8} (k_1 a)^2 \left[\frac{\rho_2}{\rho_1} - 1 + 2 \left(\frac{\mu_1 - \mu_2}{\mu_1 + \mu_2} \right) \cos(\theta - \theta_0) \right] + o((k_1 a)^2).$$
 (4.5)

The additional far-field amplitude due to the crack is $F^{(1)} = F_8^{(1)} + F_{\lambda}^{(1)}$, which follows from (2.26), (2.36) and (4.3) as

$$F^{(1)}(\theta, \theta_0) = A \frac{i}{2} \frac{(k_1 a)^2}{(1 + \mu_1/\mu_2)} [f_S(\delta) \cos \theta \cos \theta_0 + f_A(\delta) \sin \theta \sin \theta_0] + o((k_1 a)^2),$$
(4.6)

where

$$f_{S}(\delta) = \sum_{q=1}^{\infty} \tilde{\alpha}_{q}^{(S)} J_{2q-1}(\delta), \quad f_{A}(\delta) = \sum_{q=1}^{\infty} \tilde{\alpha}_{q}^{(A)} J_{2q}(\delta).$$
 (4.7a, b)

Coussy (1982) obtained an expression for the far-field pattern in the long wavelength limit by solving the static problem using complex variable methods. The same technique can also be used to calculate the long wavelength scattering from a rigid elliptic fibre partially debonded from the matrix (Coussy, 1986). Comparison of the far-field pattern F of (4.5) and (4.6) with that of Coussy (1982) yields

$$f_{\rm S}(\delta) = 1 - \cos^4\left(\frac{\delta}{2}\right), \quad f_{\rm A}(\delta) = \sin^4\left(\frac{\delta}{2}\right).$$
 (4.8a, b)

We have checked the equivalence of f_s and f_A given by (4.8) with the values defined by (4.2), (4.4) and (4.7) by numerically solving truncated versions of (4.4). The computations agree to within the degree of numerical accuracy possible.

The behaviour of F, given by (4.5), (4.6) and (4.8), as a function of δ has been discussed by Coussy (1982). For arbitrary δ ,

$$F(\theta, \theta_0) = A \frac{i}{4} (k_1 a)^2 \left[\frac{1}{2} \left(\frac{\rho_2}{\rho_1} - 1 \right) + \left(1 - \frac{2\mu_2}{\mu_1 + \mu_2} \cos^4 \frac{\delta}{2} \right) \cos \theta \cos \theta_0 \right.$$

$$\left. + \left(1 - \frac{2\mu_2}{\mu_1 + \mu_2} \left(1 - \sin^4 \frac{\delta}{2} \right) \right) \sin \theta \sin \theta_0 \right] + o((k_1 a)^2), \quad (4.9)$$

and in particular, as $\delta \to \pi$,

$$F(\theta, \theta) = A \frac{i}{8} (k_1 a)^2 \left[\frac{\rho_2}{\rho_1} - 1 + 2\cos(\theta - \theta_0) \right] + o((k_1 a)^2). \tag{4.10}$$

The monopole term in (4.10) is proportional to $(\rho_2 - \rho_1)$, and is unchanged by the presence of the debond. The dipole term however, becomes the same as the dipole

field scattered from a cylindrical void, $\mu_2 = 0$ in (4.5). Thus, as the fibre becomes almost completely disconnected from the matrix, it behaves for purposes of shear deformation exactly like a void. The inertial effects of the fibre are unaltered because, even as the width of the neck connecting the fibre to the matrix shrinks to zero, the fibre continues to oscillate in phase with the matrix.

The scattering cross-section follows from (4.9) as

$$\sigma(\omega) = |A|^2 k_1^3 a^4 \frac{\pi^2}{2} \left\{ \frac{1}{2} \left(\frac{\rho_2}{\rho_1} - 1 \right)^2 + \left(1 - \frac{2\mu_2}{\mu_1 + \mu_2} \cos^4 \frac{\delta}{2} \right)^2 \cos^2 \theta_0 + \left[1 - \frac{2\mu_2}{\mu_1 + \mu_2} \left(1 - \sin^4 \frac{\delta}{2} \right) \right]^2 \sin^2 \theta_0 \right\} + o(k_1^3 a^4). \quad (4.11)$$

If the fibre is more rigid than the matrix, $\mu_2 > \mu_1$, then the presence of the debond always decreases the cross-section, as long as $\mu_1/\mu_2 < \cos^4 \delta/2$, see Appendix B. This condition is satisfied by a very rigid fibre, $\mu_1 \ll \mu_2$, for almost all values of δ , except for the case when $\delta \to \pi$, and then σ approaches the value for the perfectly bonded fibre. Furthermore, when the fibre is perfectly rigid, the cross-section achieves an absolute minimum if $\theta_0 = 0$ and $\delta = \delta_0$, or if $\theta_0 = \pi/2$ and $\delta = \pi - \delta_0$, where $\cos^4 \delta_0/2 = 1/2$, or $\delta_0 = 65.5^0$. If the fibres are randomly oriented, then $\cos^2 \theta_0$ and $\sin^2 \theta_0$ are both replaced by 1/2 in (4.11), and a minimum cross-section is obtained for the case of a rigid fibre when $\delta = \pi/2$.

5. THE SHORT CRACK LIMIT

The general solution of Section 2 also simplies in the limit of $\delta \ll 1$, for $k_1 a = O(1)$. Then, under the substitution $v = p\delta$, (2.22) becomes

$$Q_{mn}^{(S)} \approx \int_{0}^{\infty} \frac{\mathrm{d}\nu}{\nu^{2}} J_{2m-1}(\nu) J_{2n-1}(\nu) \delta \frac{H_{\nu/\delta}^{(1)'}(k_{1}a) J_{\nu/\delta}'(k_{2}a)}{D_{\nu/\delta}}.$$
 (5.1)

By assumption, k_1a and k_2a are of order unity, therefore using the asymptotic forms of Bessel functions for large order (Abrahowitz and Stegun, 1965),

$$\delta \frac{H_{v/\delta}^{(1)'}(k_1 a) J_{v/\delta}'(k_2 a)}{D_{v/\delta}} \approx \frac{v}{k_2 a \left(1 + \frac{\mu_2}{\mu_1}\right)},\tag{5.2}$$

and so,

$$Q_{nm}^{(S)} \to \frac{1}{k_2 a \left(1 + \frac{\mu_2}{\mu_1}\right)} \frac{\delta_{mn}}{2(2n-1)}.$$
 (5.3)

Similarly, from (2.34)

$$Q_{mn}^{(A)} \to \frac{1}{k_2 a \left(1 + \frac{\mu_2}{\mu_1}\right)} \frac{\delta_{mn}}{4n}.$$
 (5.4)

The vectors $N^{(S)}$ and $N^{(A)}$ of (2.23) and (2.35) simplify in the same limit to

$$N_n^{(S)} = \frac{\delta}{2} \delta_{n_1} \sum_{p=0}^{\infty} J_p'(k_2 a) B_p^{(S)} + O(\delta^2), \tag{5.5a}$$

$$N_n^{(\Lambda)} = O(\delta^2), \quad n = 1, 2, 3, \dots$$
 (5.5b)

The COD coefficients are therefore

$$\alpha_n^{(S)} = \alpha_1^{(S)} \delta_{n1}, \quad \alpha_n^{(A)} = 0,$$
 (5.6a, b)

where

$$\alpha_1^{(S)} = \delta k_2 a \left(1 + \frac{\mu_2}{\mu_1} \right) \sum_{p=0}^{\infty} J_p'(k_2 a) B_p^{(S)}.$$
 (5.7)

Note that the COD involves only the first Chebyshev function $\phi_1^{(s)}(\theta) = (1 - \theta^2/\delta^2)^{1/2}$. Let $b = a\delta$ and $x = a\theta$, then the COD follows from (2.18) and (5.7) as

$$\Delta U = \sigma^{\text{app}} \left(\frac{1}{\mu_1} + \frac{1}{\mu_2} \right) (b^2 - x^2)^{1/2}. \quad |x| < b, \tag{5.8}$$

where σ^{app} is the applied normal stress on the crack face due to the quasistatic field about the small crack,

$$\sigma^{\text{app}} = \mu_2 \frac{\partial}{\partial r} u_2^{(0)}(r, 0), \quad r = a. \tag{5.9}$$

The crack experiences a quasistatic opening since $k_1b \ll 1$, even though the fibre is in a fully dynamic state, i.e. $k_2a = O(1)$. It may be verified independently that (5.8) is in fact the COD on a flat interfacial crack between half spaces of moduli μ_1 and μ_2 subject to loading σ^{app} at infinity.

The additional radiation generated by the small crack is

$$F^{(1)}(\theta,\theta_0) = \frac{\mathrm{i}}{4(1+\mu_1/\mu_2)} \frac{(k_1 a \delta)^2}{(1+\mu_1/\mu_2)} g,\tag{5.10}$$

where g is for plane wave incidence (see Appendix A),

$$g = \frac{1}{A} \left[\frac{k_2}{2k_1} \left(1 + \frac{\mu_2}{\mu_1} \right) \right]^2 \left(\sum_{p=0}^{\infty} J_p'(k_2 a) B_p \cos p \theta_0 \right)$$

$$\times \left(\sum_{q=0}^{\infty} (-1)^q J_q'(k_2 a) B_q \cos q\theta\right). \quad (5.11)$$

As $k_1 a \to 0$, $g \to A \cos \theta \cos \dot{\theta}_0$, and so (5.10) agrees with (4.6) and (4.8) in the double

limit of $\delta \ll 1$, $k_1 a \ll 1$. The factor g of (5.11) becomes in the limit of a rigid fibre, $\mu_1/\mu_2 \ll 1$, $k_1/k_2 = O(1)$,

$$g \to \frac{-A}{(\pi k_1 a)^2} \left(\sum_{p=0}^{\infty} \varepsilon_p \, \mathbf{i}^p \frac{\cos p \theta_0}{H_p^{(1)}(k_1 a)} \right) \left(\sum_{q=0}^{\infty} \varepsilon_q (-\mathbf{i})^q \frac{\cos q \theta}{H_q^{(1)}(k_1 a)} \right). \tag{5.12}$$

In general, it follows from (3.6) and (5.10) that the presence of the small debond produces a change of order δ^2 in the scattering cross-section.

THE STRESS INTENSITY FACTOR

The static stress intensity factor, KI_s , is defined as

$$KI_{s} = \lim_{\theta \to \delta_{+}} \left[(2r')^{1/2} \tau_{rz} \right]_{r=a}$$

$$= -\lim_{\theta \to \delta_{-}} \frac{\mu_{1} \mu_{2}}{\mu_{1} + \mu_{2}} \frac{\Delta U(\theta)}{(2r')^{1/2}} \bigg|_{r=a},$$
(6.1)

where r' is the radial distance from the tip at $\theta = \delta$. Tamate and Yamada (1969) derived the static stress intensity factor for a uniform antiplane stress τ_0 at infinity, which is inclined at the angle θ_0 ,

$$KI_{\rm s} = -\frac{2\mu_2}{\mu_1 + \mu_2} \tau_0 (a \sin \delta)^{1/2} \cos \left(\theta_0 - \frac{\delta}{2}\right). \tag{6.2}$$

We define the dynamic stress intensity factor KI_d , by analogy with (6.1), as

$$KI_{d} = -\lim_{\theta \to \delta_{-}} \frac{\mu_{1} \mu_{2}}{\mu_{1} + \mu_{2}} \frac{\Delta U(\theta)}{(2r')^{1/2}} \bigg|_{r=\theta}.$$
 (6.3)

From (2.18), as $\theta \rightarrow \delta_{-}$,

$$\Delta U_{\rm S}(\theta) = \left[2\left(1 - \frac{\theta}{\delta}\right)\right]^{1/2} \sum_{n=1}^{\infty} (-1)^{n-1} \alpha_n^{\rm (S)},\tag{6.4}$$

and therefore the symmetric dynamic stress intensity factor is

$$KI_{\rm d}^{\rm (S)} = \frac{1}{(a\delta)^{1/2}} \frac{\mu_1 \mu_2}{\mu_1 + \mu_2} \sum_{n=1}^{\infty} (-1)^n \alpha_n^{\rm (S)}. \tag{6.5}$$

This should agree in the low frequency limit with the symmetric part of (6.2)

$$KI_s^{(S)} = -\frac{2\mu_2}{\mu_1 + \mu_2} \tau_0(a\sin\delta)^{1/2} \cos\theta_0 \cos\frac{\delta}{2},\tag{6.6}$$

where from (2.5), $\tau_0 = ik\mu_1 A$. Similar expressions can be obtained for the antisymmetric dynamic stress intensity factor.

7. Numerical Results and the Low Frequency Resonance

Numerical results for the scattering cross-section and the far-field radiation pattern have been computed for two combinations of matrix and fibre: (i) epoxy, $\mu_1 = 1.28$ GPa, $\rho_1 = 1.25$ g/cc, and glass, $\mu_2 = 29.9$ GPa, $\rho_2 = 2.55$ g/cc; and (ii) aluminium, $\mu_1 = 26.49$ GPa, $\rho_1 = 2.70$ g/cc, and tungsten, $\mu_2 = 155.47$ GPa, $\rho_2 = 19.19$ g/cc. The results are for plane wave incidence, and were obtained by solving truncated versions of (2.11)–(2.23) and (2.33)–(2.35). The computations were validated by (i) increasing the truncation limit and checking that the difference was negligible, and (ii) numerically verifying that the optical theorem (3.6) was always satisfied.

The exact scattering cross-section and long wavelength approximation are compared in Fig. 2 for glass/epoxy, $\delta = 130^{\circ}$ and $\theta_0 = 0$. The approximate theory is extremely accurate for k_1a less than 0.2, but the peak at k_1a near 0.6 clearly indicates that the quasistatic analysis is breaking down. The peak becomes more pronounced and occurs at lower frequencies as the crack size is increased, see Fig. 3, until as $\delta \rightarrow \pi$, the shape of the peak becomes more and more like that of a sharp resonance. In particular, for $\delta = 179.9^{\circ}$ the resonance occurs at about $k_1 a = 0.2$, which is right in the range of k_1a for which one would expect the quasistatic theory to apply. The probable explanation for the resonance is that as $\delta \to \pi$ the narrow neck joining the fibre and matrix permits large relative motion to occur. The neck, in other words, has a smaller and smaller stiffness as $\delta \to \pi$. The resonance is then caused by relative motion of the matrix and fibre in opposite senses. The resonance frequency is determined by the neck stiffness, which goes to zero, and the inertia of the fibre and matrix, which remain relatively constant independent of δ . This hypothesis is explored in Appendix C, where a simple model is presented for this low frequency resonance. The model involves a single free parameter related to the unknown inertia of the matrix as it oscillates. We found that the positions of the peaks in Fig. 3 and for other values of δ could be well matched by setting the parameter as $\beta = 5.13$, with comparisons

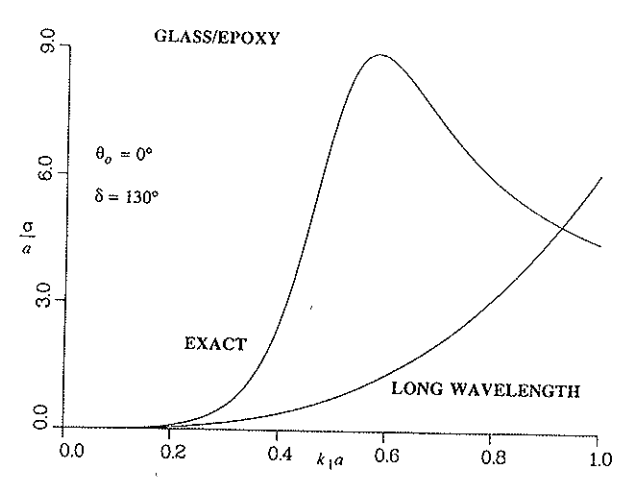


Fig. 2. Comparison of the exact and approximate scattering cross-section for glass/epoxy, $\delta = 130^{\circ}$ and $\theta_0 = 0$.



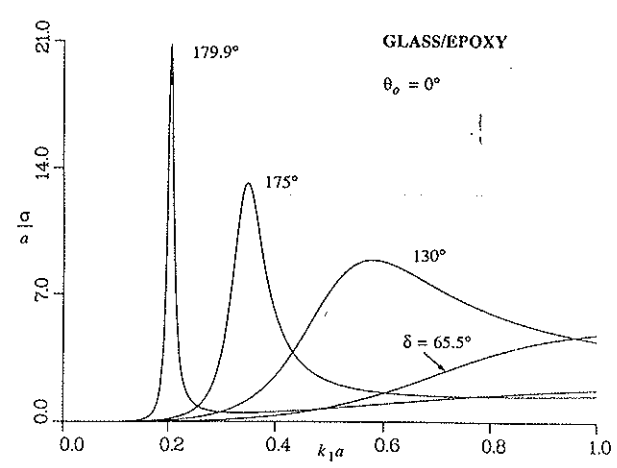


Fig. 3. The exact cross-section for glass/epoxy with $\theta_0 = 0$ and $\delta = 65.5^{\circ}$, 130°, 175° and 179.9°.

as shown in Fig. 4 for glass/epoxy. The agreement between the simple model and the exact results is very convincing and suggests that a slightly more sophisticated quasistatic analysis might capture the full resonance phenomenon, although we will defer consideration of this until a later date. In the meantime, we note that the low frequency resonance is also evident for the tungsten/aluminium combination, see Fig. 5. The positions of the peaks in Fig. 5 are at lower value of k_1a than for glass/epoxy in Fig. 3, which may be attributed to the greater densities of tungsten and aluminium. Finally, we note the connection between the low frequency resonance and the Helmholtz resonance of an acoustic cavity (RAYLEIGH, 1945). The acoustic resonance is caused by the compressibility of the cavity fluid and the inertia of the fluid in the

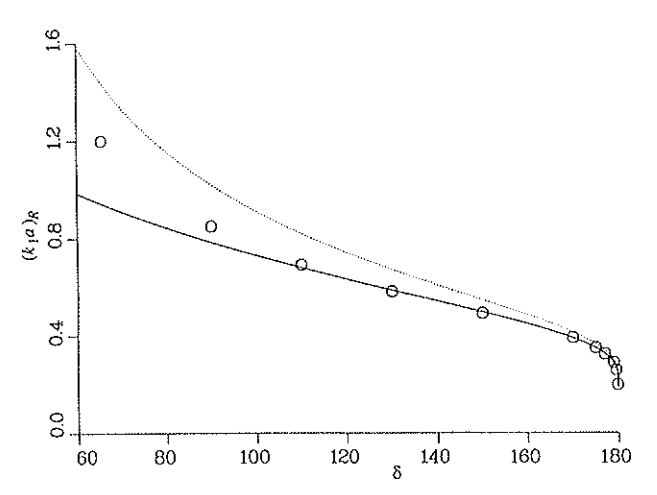


Fig. 4. Comparison of the low frequency resonance frequency vs δ . The solid and dashed curves are from Appendix C, Eqs C(10) and (C11), respectively, with $\beta = 5.13$, and the circles are from the exact computed cross-sections.

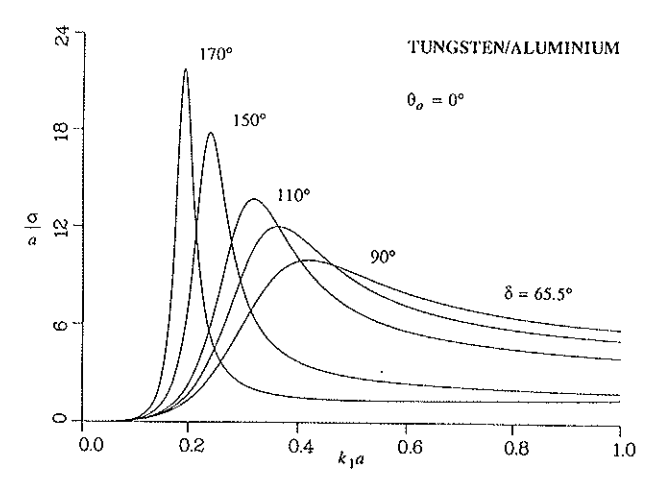


Fig. 5. The cross-section for tungsten/aluminium with $\theta_0 = 0$ and $\delta = 65.5^{\circ}$, 90° , 110° , 150° and 170° .

neck joining the cavity to the exterior medium. The roles of the "cavity" material and the material in the neck are reversed in the present problem. Thus, the inertia may be attributed to the gross motion of the fibre, while the spring constant is governed by the elastic strain in the vicinity of the neck. The main distinction between the two phenomena is due to the different boundary conditions on the cavity and fibre, respectively. The behaviour of the low frequency resonance is shown in Fig. 6 for $\delta = 170^{\circ}$ and different directions of incidence.

The behaviour of the cross-section at higher frequencies is illustrated in Fig. 7. The curves for a uniformly bonded fibre, $\delta=0$, and a void are shown for comparison. It is worth noting that even for $\delta=170^\circ$ the cross-section is quite unlike that for the void. Figures 8, 9 and 10 illustrate the far-field radiation pattern for glass/epoxy for

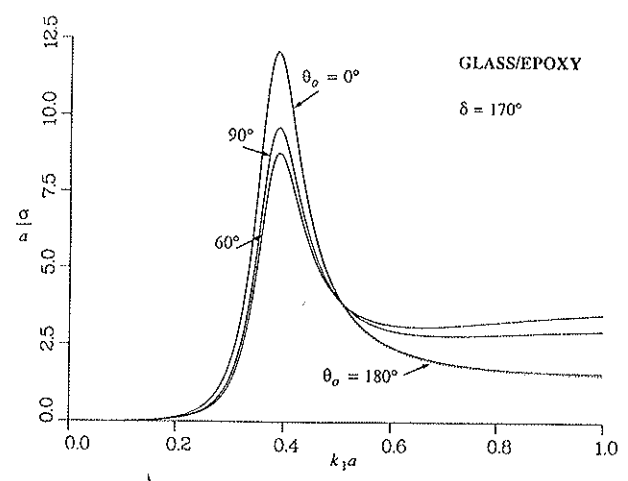


Fig. 6. The low frequency resonance for glass-epoxy with $\delta = 170^{\circ}$, and $\theta_0 = 0$, 60° , 90° and 180° (dotted curve).

....

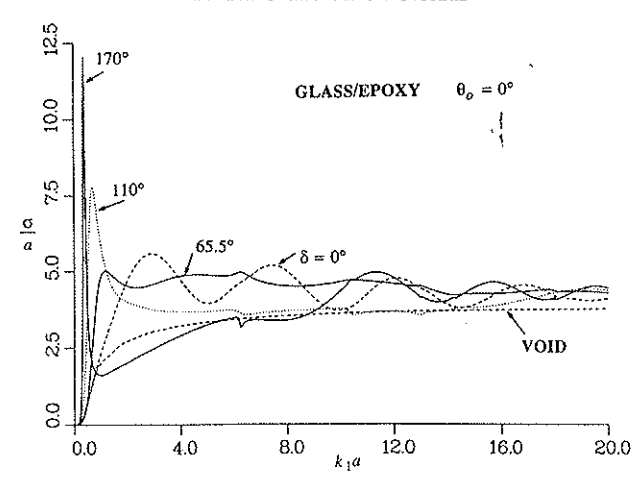


Fig. 7. The cross-section for glass/epoxy, $\theta_0=0$, $\delta=0$, 65.5°, 110° and 170°. The curve for an empty void is shown for comparison.

different frequencies and angles of incidence. In Fig. 8 the pattern is shown for the frequency of the resonance and for neighbouring frequencies where the resonance is not as significant. Quasistatic theory predicts that at the frequencies involved the patterns should have monotonically increasing magnitudes, which is clearly not the case from Fig. 8.

Finally, the static and dynamic stress intensity factors are illustrated in Figs 11 and 12. Note in particular the magnification of the stress intensity at the low frequency

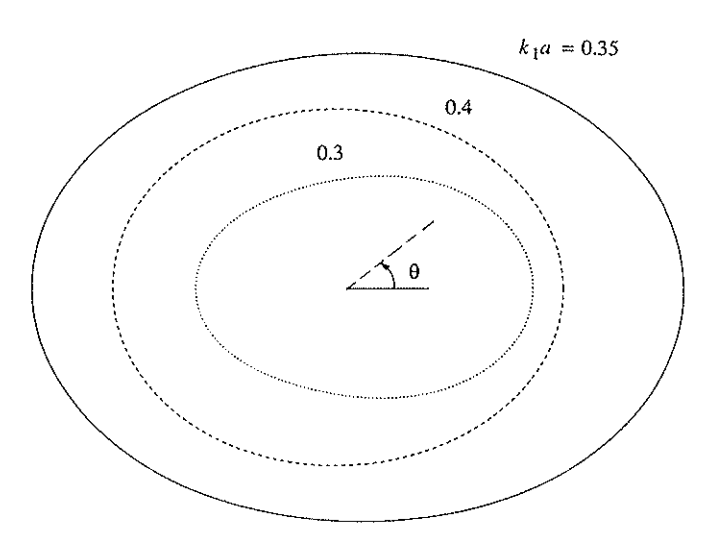


Fig. 8. The far-field pattern for glass/epoxy with $\delta = 175^{\circ}$, $\theta_0 = 0$, at the low frequency resonance, $k_1 a = 0.35$, and slightly off resonance, $k_1 a = 0.3$ and $k_1 a = 0.4$.

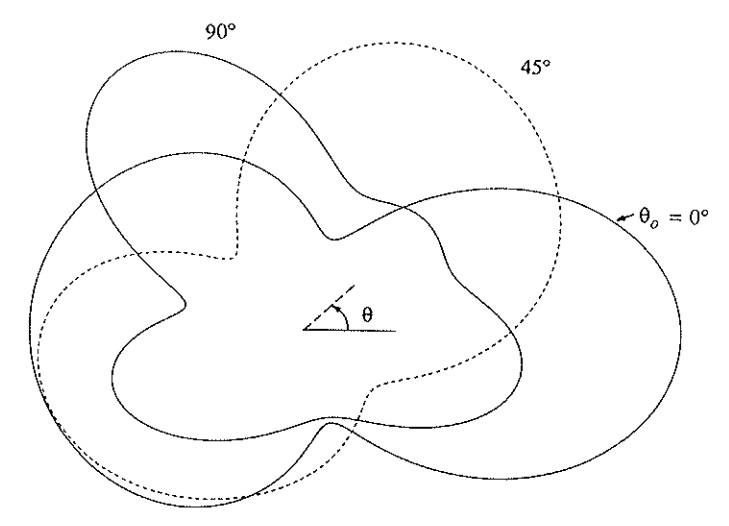


Fig. 9. The same as Fig. 8 but for $\delta = 90^{\circ}$, $\theta_0 = 0$, 45° and 90°, $k_1 a = 2.0$.

resonance in Fig. 12, to be compared with Fig. 2. The change in phase of the complex-valued stress intensity factor near this frequency is characteristic of a resonance phenomenon.

8. Discussion

Ultrasonic inspection of composite materials is normally made at frequencies such that k_1a is small, i.e. the wavelength greatly exceeds the fibre radius. If c is the volume fraction of fibres in the composite, then the quasistatic approximation of Section 4

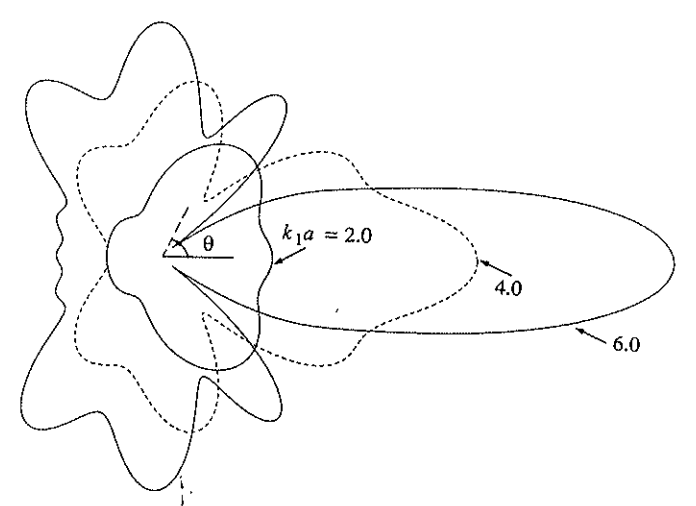


Fig. 10. The far-field patterns for glass/epoxy with $\delta = 175^{\circ}$, $k_1 a = 2.0$, 4.0 and 6.0.

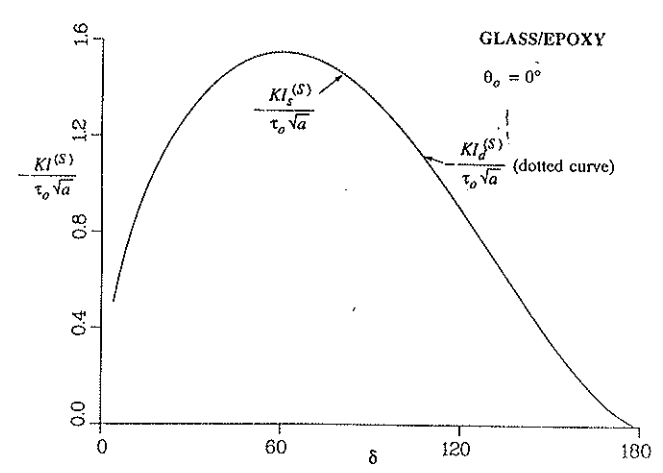


Fig. 11. A comparison of the symmetric stress intensity factor in the static limit. KI_s is given by (6.6) and KI_d is computed from (6.5) using the static COD coefficients $\alpha_n^{(S)}$ of (4.3a).

predicts an attenuation of $\alpha = cEk_1^3a^2$, where E is a material constant and follows from (4.11) as $E = E(\mu_2/\mu_1, \rho_2/\rho_1, \theta_0, \delta)$ for a single fibre. In general, the fibres will have a distribution in values of θ_0 and δ , and E must be averaged accordingly. If, however, the fibre debonds are all similar, then careful measurement of the attenuation for several distinct propagation directions should provide sufficient information to determine δ and θ_0 . This type of inverse measurement is fraught with difficulties since it requires looking for small differences in the slope of the low frequency attenuation. In addition, the background attenuation in the absence of fibre debonds may not be so well defined, due to other damping mechanisms.

The numerical results for the low frequency scattering cross-section and the simple model of Appendix C indicate the possibility of a strong low frequency resonance

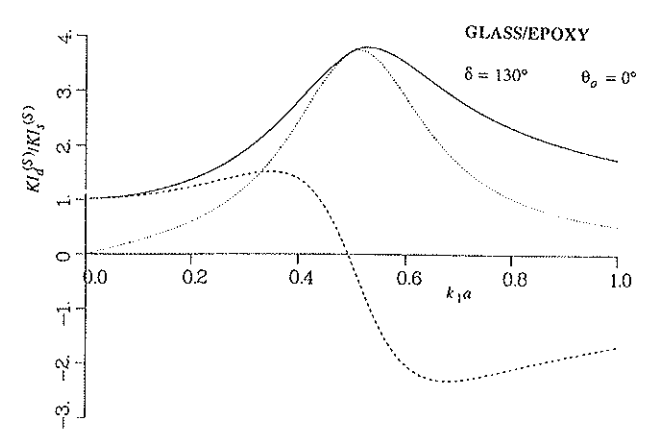


Fig. 12. The complex-valued dynamic stress intensity factor from (6.5), normalized with respect to the static value, KI_s . The solid curve is the absolute value, the dashed curve the real part, and the dotted curve the imaginary part.

when the debond becomes large. The associated attenuation will be significantly enhanced by this resonance. For example, as Fig. 3 shows for a glass/epoxy system, the attenuation at very low frequencies can be increased by orders of magnitude. In contrast, the quasistatic theory predicts that the debond reduces the stiffening effect of the fibre, and leads to a decrease in attenuation.

In conclusion, it is suggested that the presence of strong low frequency resonances and the associated increase in ultrasonic attenuation could provide unambiguous evidence of debonding. A similar resonance phenomenon is expected for longitudinal and SV incident waves and will be explored in a subsequent publication.

ACKNOWLEDGEMENTS

The authors would like to thank Prof. W. J. BOTTEGA for his useful suggestions. This work was supported by the National Science Foundation through Grant. No. MSM86-16256.

REFERENCES

ABRAMOWITZ, M. and	1965	Handbook of Mathematical Functions. Dover, New
Stegun, I. A.		York.
Beltzer, A. I.	1988	Acoustics of Solids. Springer, New York.
Boströм, А.	1987	J. appl. Mech. 54, 503.
Coussy, O.	1982	C.R. Acad. Sci. Paris 295, 1043.
Coussy, O.	1984	Wave Motion 6, 223.
Coussy, O.	1986	
Krenk, S. and	1982	
Schmidt, H.		
NEERHOFF, F. J.	1979	Appl. Sci. Res. 35, 237.
RAYLEIGH, J. W. S.	1945	The Theory of Sound, Vol. II. Dover, New York.
TAMATE, O. and	1969	Tech. Reports Tohoku Univ. 34, 161.
YAMADA, T.		Town step of the stational office off 101.

APPENDIX A: SCATTERED FIELDS FOR A PERFECTLY BONDED FIBRE

The incident plane wave (2.5) can be rewritten

$$u^{\rm in} = A \sum_{n=0}^{\infty} \varepsilon_n i_n^n J_n(k_1 r) \cos n(\theta - \theta_0), \tag{A1}$$

where

$$\varepsilon_n = \begin{cases} 1, & n = 0 \\ 2, & n \neq 0 \end{cases} \tag{A2}$$

and J_n are Bessel functions. Let

Y. YANG and A. N. NORRIS

$$u_1^{(0)} = \sum_{n=0}^{\infty} A_n H_n^{(1)}(k_1 r) \cos n(\theta - \theta_0),$$
 (A3a)

$$u_2^{(0)} = \sum_{n=0}^{\infty} B_n J_n(k_2 r) \cos n(\theta - \theta_0),$$
(A3b)

where $H_n^{(1)}$ are Hankel functions of the first kind. Standard analysis (e.g. Beltzer, 1988) yields

$$A_n = A \frac{\varepsilon_n i^n}{D_n} [Z J_n(k_1 a) J'_n(k_2 a) - J'_n(k_1 a) J_n(k_2 a)], \tag{A4a}$$

$$B_n = \frac{A\varepsilon_n 2 i^{n+1}}{\pi k_1 a D_n},\tag{A4b}$$

where

$$D_n = H_n^{(1)'}(k_1 a) J_n(k_2 a) - Z H_n^{(1)}(k_1 a) J_n'(k_2 a), \tag{A5}$$

$$Z = \frac{\mu_2 k_2}{\mu_1 k_1}.$$
(A6)

The coefficients $B_n^{(S)}$ and $B_n^{(A)}$ of (2.16) and (2.29) are therefore

$$B_n^{(S)} = B_n \cos n\theta_0, \quad n = 0, 1, 2, \dots,$$
 (A7a)

$$B_n^{(\Lambda)} = B_n \sin n\theta_0, \quad n = 1, 2, \dots$$
 (A7b)

and the far-field pattern is

$$F^{(0)}(\theta, \theta_0) = \frac{1}{2\pi} \sum_{n=0}^{\infty} i^{-n} A_n \cos n(\theta - \theta_0).$$
 (A8)

APPENDIX B: THE QUASISTATIC CROSS-SECTION

It is clear from (4.11) that for fixed frequency the difference $\sigma - \sigma^{(0)}$ between the cross-section with the debond and the cross-section $\sigma^{(0)}$ for the perfectly bonded fibre is proportional to, and of the same sign as

$$\frac{\mu_1}{\mu_2} + \cos^4 \frac{\delta}{2} \left(\cos^4 \frac{\delta}{2} - 1 - \frac{\mu_1}{\mu_2} \right) \cos^2 \theta_0 - \left(1 - \sin^4 \frac{\delta}{2} \right) \left(\frac{\mu_1}{\mu_2} + \sin^4 \frac{\delta}{2} \right) \sin^2 \theta_0.$$
 (B1)

A simple examination of (B1) shows that three possibilities exist:

(i)
$$\sigma < \sigma^{(0)}$$
 for all θ_0 if $\frac{\mu_1}{\mu_2} < \cos^4 \frac{\delta}{2}$, (B2)

(ii)
$$\sigma > \sigma^{(0)}$$
 for all θ_0 if $\frac{\mu_1}{\mu_2} > 1 - \sin^4 \frac{\delta}{2}$, (B3)

(iii) if
$$\cos^4 \frac{\delta}{2} < \frac{\mu_1}{\mu_2} < 1 - \sin^4 \frac{\delta}{2}$$
,

then $\sigma > \sigma^{(0)}$ for $0 \le \theta_0 < \phi_0$, and $\sigma < \sigma^{(0)}$ for $\phi_0 < \theta_0 \le \pi/2$, where

Shear wave scattering from a debonded fibre

$$\tan^2 \phi_0 = \left[\frac{1 - \cos^4 (\delta/2)}{\sin^4 (\delta/2)} \right] \left[\frac{\mu_1/\mu_2 - \cos^4 (\delta/2)}{1 - \sin^4 (\delta/2) - \mu_1/\mu_2} \right].$$
 (B4)

APPENDIX C: THE LOW FREQUENCY RESONANCE

Consider an isolated fibre of radius a, density ρ and shear modulus μ . The fibre is in static equilibrium under the combination of a force F along its axial direction and uniformly distributed over the cross-section, and an equal but opposite force applied on the side of the fibre over the "neck" $-\varepsilon < \theta < \varepsilon$, where $\varepsilon = \pi - \delta$. The axial displacement satisfies

$$\frac{1}{r}\frac{\partial}{\partial r}\left(r\frac{\partial}{\partial r}w\right) + \frac{1}{r^2}\frac{\partial^2 w}{\partial \theta^2} + 2B = 0, \quad r < a, \quad -\pi < \theta < \pi, \tag{C1}$$

where

$$B = \frac{F}{2\pi a^2 \mu}.$$
(C2)

293

The general solution to (C1) which is symmetric about $\theta = 0$ is

$$w = A_0 - \frac{B}{2}r^2 + \sum_{n=1}^{\infty} A_n r^n \cos n\theta.$$
 (C3)

The shear force on the side of the fibre is

$$\mu \frac{\partial w}{\partial r}(a, \theta) = \begin{cases} 0, & |\theta| > \varepsilon, \\ -\frac{F}{a}f(\theta), & |\theta| < \varepsilon, \end{cases}$$
(C4)

where the exact form of the distributed shear force is specified by $f(\theta)$ which is symmetric, $f(-\theta) = f(\theta)$, and $f_0 = 1$, where

$$f_n = \int_{-\varepsilon}^{\varepsilon} f(\theta) \cos n\theta \, d\theta. \tag{C5}$$

Equations (C3)-(C5) imply

$$A_n = -\frac{2}{n}a^{2-n}Bf_n, \quad n = 1, 2, 3, \dots$$
 (C6)

Finally, we specify the rigid body displacement by imposing the condition w(a, 0) = 0, which means that

$$A_0 = Ba^2 \left(\frac{1}{2} + 2 \sum_{n=1}^{\infty} \frac{f_n}{n} \right). \tag{C7}$$

An elastic stiffness K may be defined by

$$K = \frac{F}{\tilde{w}},$$
 (C8)

where $\bar{w} = A_0 - Ba^2/4$ is the average displacement of the fibre in the direction of the force. The low frequency resonance is hypothesized as a spring-mass type of resonance in which the stiffness is approximately the same as K, and the mass is $m = \beta^2 \rho \pi a^2$, where β is a number larger than unity which accounts for the inertia of the material outside the fibre. The resonance frequency is $\omega_R = (K/m)^{1/2}$, and the nondimensional resonance frequency analogous to $k_2 a$, is $\chi_R = \omega_R a/c$, where $c = (\mu/\rho)^{1/2}$. Thus

Y. YANG and A. N. NORRIS

$$\chi_{\rm R} = \beta^{-1} \left(\frac{1}{8} + \sum_{n=1}^{\infty} \frac{f_n}{n} \right)^{-1/2}.$$
(C9)

The coefficients f_n , $n=1, 2, 3, \ldots$, depend upon the distribution of shear force across the neck. If this is uniform, then (C5) with $f=1/(2\varepsilon)$ yields

$$f_n = \frac{\sin n\varepsilon}{n\varepsilon}.$$
 (C10)

A more realistic distribution, which has the correct stress singularity at the crack tips, is $f(\theta) = \pi^{-1} (\epsilon^2 - \theta^2)^{-1/2}$, for which

$$f_n = J_0(n\varepsilon). (C11)$$